Electronic Journal of Structural Engineering

Original Article

Cite this: DOI:10.56748/ejse.24618

Received Date:12 April 2024
Accepted Date: 10 August 2024

1443-9255
https://ejsei.com/ejse

Study on Stress Characteristics Response of Submarine Shield Segment Under Ultra-High-Water Pressure

Bing Li[a], Kaichen Ying[b]*,Liupan Dou[b], Yuxiang Xing[b], Fang Yong[b]
[a] China Railway 14th Bureau Group Shield Engineering Co., Ltd., Nanjing, 211800, China.
[b] Key Laboratory of Transportation Tunnel Engineering, Ministry of Education, Southwest Jiaotong University, Chengdu, 610031, China.
*Corresponding author: 1051098250@qq.com

Abstract

In the construction and operation stage of shield tunnel, clarifying the mechanical characteristics of the overall structure is crucial for ensuring shield tunnel safety. In this paper, the shell-spring model is established by ABAQUS finite element software for the ultra-high water pressure submarine shield tunnel. The mechanical behavior of shield segment structure under varying water pressure, different key block position and different strata is studied and analyzed. The results show that at the same segment assembly position, the axial force of the segment increases greatly with the increase of water pressure, and the growth rate is as high as 150 %. The internal force of the segment is mainly axial force. Under the ultra-high-water pressure, the corresponding position of the maximum deformation of the segment is related to the position of the segment joint at the arch bottom. In the staggered assembly, the axial force fluctuation near the arch bottom is larger than that of the straight assembly, and the peak bending moment and the maximum axial force are near the invert. In addition, near the 120 degrees of the vault, the bending moment oscillates obviously near the joint in the stratum with small coefficient of soil reaction. The larger the coefficient of soil reaction is, the more uniform the axial force of the whole segment is. The research results provide a theoretical insight for the optimization design of shield tunnel segments.

Keywords

Tunnel engineering, Shield tunnel, Ultra-high-water pressure, Shell-spring model, Structural internal force

1. Introduction

When the cross-river tunnel is constructed, the shield segment is subjected to huge water and soil pressure, and the design and construction are faced with major technical problems (Sun et al., 2023; S. Zhang et al., 2023). The shield tunnel is assembled by multiple segments, with segment joints particularly susceptible as weak points in the lining. The design of segment assembly method is critical in ultra-high water pressure conditions, impacting their mechanical properties (X. Liu et al., 2022) and plays an important role in the safety of segment structure (Liu et al., 2023).

Based on the Tunnel Association's investigation, current methods for calculating internal forces in shield tunnel segments include the homogeneous ring method, modified routine method, multi-hinge ring method, and beam-spring model (J. Liu et al., 2022). Scholars have often adjusted lining joint parameters using the beam-spring model (Lei et al., 2018; Yang et al., 2022), and developed the beam-joint model based on this framework (Zhu et al., 2019). However, the above models are two-dimensional analysis models, so they cannot reflect the phenomenon of stress concentration at the edge of the segment. In addition, the segment lining is a cylindrical structure, which is assembled by many segments. The traditional two-dimensional model often struggles to accurately depict the interactions among lining rings, leading to discrepancies with the actual mechanical behavior of the structure. Achieving longitudinal calculations in practical scenarios proves challenging with this approach. Recognizing these limitations, scholars have explored alternative models to address these deficiencies and better analyze the spatial stress characteristics of lining structures under complex construction conditions, such as the shell-elastic hinge model considering the bending stiffness of the longitudinal joint (Hu et al., 2005), and the shell-spring model considering the bending, shear and tensile stiffness of the longitudinal joint. These advancements aim to provide more accurate representations of segmental behavior in shield tunnels. Researchers have extensively examined the applicability of various models, focusing on factors such as longitudinal and circumferential joint stiffness (rotational and shear stiffness) and segment assembly methods (Guan et al., 2015; Huang et al., 2019; Kavvadas et al., 2017). Among these models, the shell-spring calculation model offers notable advantages over the beam-spring model. However, it still exhibits shortcomings in the joint system (Kou et al., 2021; Liu et al., 2021; Xu et al., 2019). These deficiencies include neglecting segment stiffness directionality, overlooking longitudinal deformation issues, and using joint parameters that may not align with real-world conditions. To address these concerns, researchers have established the mechanical model of the segment joint according to the joint structure (Feng et al., 2021; L. Zhang et al., 2023; Zhong et al., 2006). Yan et al. (Yan et al., 2019) developed a three-dimensional shell spring model, and used the automatic iteration of the joint bending stiffness to reflect the nonlinear characteristics of the joint bending stiffness. However, this kind of nonlinear joint stiffness determination mode is usually used in the internal force analysis of lining with solid model, which has the characteristics of detailed modeling, large calculation amount and poor convergence.

To elucidate the impact of ultra-high-water pressure on the load characteristics of shield segment linings, this study draws on the engineering context of the shield section in the Pearl River Estuary Tunnel of the Shenjiang Railway. Using ABAQUS finite element software, an analysis model is constructed to investigate the mechanical characteristics of shield segment structures under conditions of ultra-high-water pressure, staggered assembly configurations, and stratum characteristics, and uncover how water pressure influences the mechanical properties of segment structures.

2. Project Overview

This paper focuses on research conducted within the context of the Pearl River Estuary Tunnel of the Shenzhen-Jiangmen Railway. The Shenjiang Railway route spans from Shenzhen Xili Station in the east through various districts including Nanshan and Bao'an in Shenzhen, Humen Town and Binhai New Area in Dongguan, Nansha District in Guangzhou, and Jianghai and Xinhui Districts in Jiangmen, ending at Jiangmen Station with a total length of 116.12 km. The Pearl River Estuary Tunnel specifically connects Dongguan Humen and Guangzhou Nansha, spanning a total length of 13.69 km.as shown in Fig. 1. Notably, this tunnel holds the record for the deepest underwater burial depth in China at 115 m, resulting in the highest water pressure for a shielded section globally, reaching 1.06 MPa.

The tunnel is designed as a single-hole double-line, with an inner diameter of 11.7 m, a width of 2.0 m, and an effective clearance of 74.05 m2. The thickness of the segment on the Humen side is 600 mm, and the corresponding outer diameter is 12.9 m. Each segment adopts a standard general-shaped ring configuration, with each segment spanning a central angle of 40°. Each ring is composed of standard blocks (B1 ~ B6) adjacent blocks (L1, L2) and key blocks (F), as illustrated in Fig. 2(a). There are 36 bolts in the longitudinal direction of the segment ring and 27 bolts in the circumferential direction. The concrete lining ring is assembled in a staggered configuration, offering 10 distinct basic assembly positions, which are illustrated in Fig. 2(b).

Fig. 1 Plane location of Pearl River Estuary Tunnel

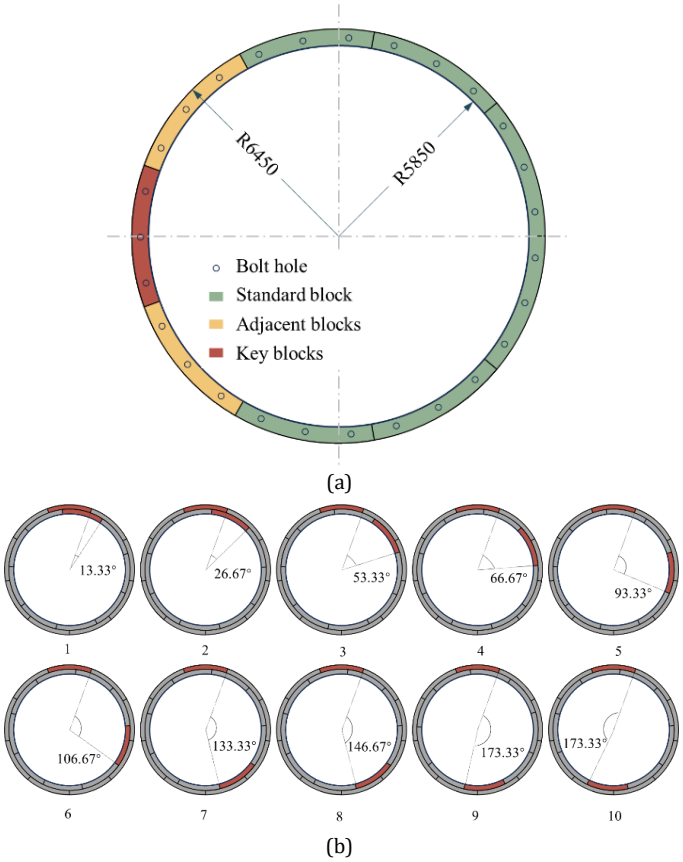

Fig. 2 Shield tunnel segment design, (a) Segment size, (b) Stagger assembly segment position

3. Numerical Model

3.1 Segment calculation model

In the current commonly used shield lining segment design model, the modified routine model cannot reflect the influence of the joint on the structural force. The multi-hinge ring method cannot reflect the effect of staggered assembly. In the study of the load characteristics of the relevant segments, it is pointed out that the shell spring model can truly reflect the situation of the whole segment ring, and in the numerical calculation, the bolt connection at the joint is simulated by the spring, and the actual mechanical behavior of the joint is simulated by the stiffness corresponding to different degrees of freedom of the circumferential joint and the longitudinal joint.

In the beam-spring model, the beam element is used to simulate the segment, so the longitudinal stress difference of the segment cannot be reflected, and only the plane strain state is reflected. The shell-spring model can solve this problem well by using curved shell elements to truly reflect the actual stress state of the segment. Therefore, this paper uses a three-dimensional shell-spring model (as shown in Fig. 3), and the mesh element type is set to S4R. The stress characteristics of shield tunnel structure under ultra-high-water pressure are analyzed. Among them, the radial and tangential spring stiffness are set between adjacent segments to simulate the inter-ring force transmission effect of the longitudinal joint, and the joint bending, compression and shear stiffness are set between each ring segment to simulate the joint force transmission.

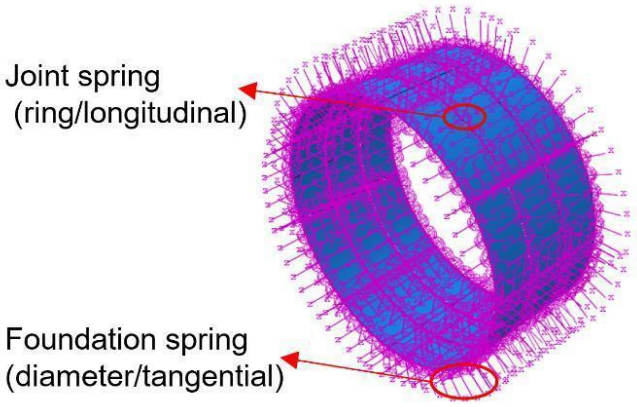

Fig. 3 Three-dimensional shell-spring model

3.2 Calculation parameters of segment design

According to the relevant engineering geological survey report, the relevant stratigraphic parameters in the calculation are listed in Table 1. The shield segment is C60 reinforced concrete material with elastic modulus of 35.5 GPa and Poisson 's ratio of 0.2.

Table 1. Main stratum property parameters of Pearl River Estuary Tunnel

Strata	Sandy gravel strongly weathered granite	Slightly weathered gravelly sandstone	Medium sand
weight (kN/m³)	19.4	25.9	20
elastic modulus (MPa)	200	20000	50
poisson 's ratio	0.25	0.23	0.3
cohesive force (kPa)	0	0	0
friction angle (°)	40	60	32
lateral pressure coefficient	0.33	0.25	0.43
coefficient of soil reaction (MPa/m)	90	250	23

The finite element software ABAQUS was used to establish the segment model for analysis. The three-dimensional shell element is used to simulate each segment. The elastic constitutive relation is selected for the concrete segment, and the effect of the bolt is simulated by setting the spring at the bolt position. According to the Eq. (1) (Huang, 2007), the stiffness of the corresponding segment joint is calculated, and the spring stiffness of the stratum around the segment is calculated according to the Eq. (2) (Arnau and Molins, 2011; Wang et al., 2011). The calculation results are shown in Table 2 and 3.

$$\begin{cases} K_t = \dfrac{Eh}{2.4(1+v)b} \\ K_r = \dfrac{E}{\left(\dfrac{b}{h}\right)^3 + \dfrac{2k(1+v)b}{h}} \\ K_n = EA/L \end{cases} \tag{1}$$

$$\begin{cases} k_r = \dfrac{3E}{R(1+v)(5-6v)} \\ k_s = \dfrac{1}{3}k_r \end{cases} \tag{2}$$

Where, E is elastic module, b is the section width, h is the section thickness, v is poisson's ratio.

Table 2. Stiffness of segment joint in numerical model

Longitudinal joint stiffness		
Bending stiffness K_θ（kN·m/rad）	Axial compressive stiffness K_n（kN/m）	Shear stiffness K_s（kN/m）
3.22×10^7	2×10^{10}	1.61×10^5
Ring joint stiffness		
Radial shear stiffness K_r（kN/m）		Tangential shear stiffness K_t（kN/m）
1.31×10^6		8.29×10^6

Table 3. Stiffness value of formation reaction spring

Strata	Radial stiffness of stratum k_r （kN/m）	Tangential stiffness of stratum k_s （kN/m）
Sandy gravel strongly weathered granite	9e-2	3e-2
Slightly weathered gravelly sandstone	2.5e-1	8.33e-2
Medium sand	2.5e-2	8.33e-3

4. Numerical Analysis

4.1 Calculated work condition

According to the study of submarine shield tunnel under different water pressure, three kinds of external water pressure of 0.2 MPa, 0.4 MPa and 0.9 MPa are taken respectively. Among them, the value corresponds to the water load value at the horizontal arch waist of the tunnel. The water load considers the influence of the vertical gradient and is applied radially to the outer surface of the segment. To reduce the influence of other factors, the simulation is unified in the same buried depth of gravelly strongly weathered granite strata. On this basis, the load characteristics of the segments under staggered assembly under ultra-high-water pressure are compared and analyzed. In addition, the influence of ultra-high-water pressure on shield tunnel structure under different strata is analyzed, including sandy gravel strongly weathered granite, slightly weathered gravelly sandstone and medium sand strata, which correspond to the same vertical earth pressure. The horizontal earth pressure and the spring stiffness of the stratum around the segment are determined by the nature of stratum property.

4.2 Analysis of mechanical properties under different water pressure

According to the change of water pressure along the Pearl River Estuary Tunnel, the external water pressure is selected as 0.2MPa, 0.4MPa and 0.9MPa respectively, and the staggered assembly method is the same. The calculation results are shown in Fig. 4. The starting point of the angle corresponds to the vault, and the axial force and bending moment data of the middle ring are extracted along the clockwise direction. The results are shown in Fig. 5.

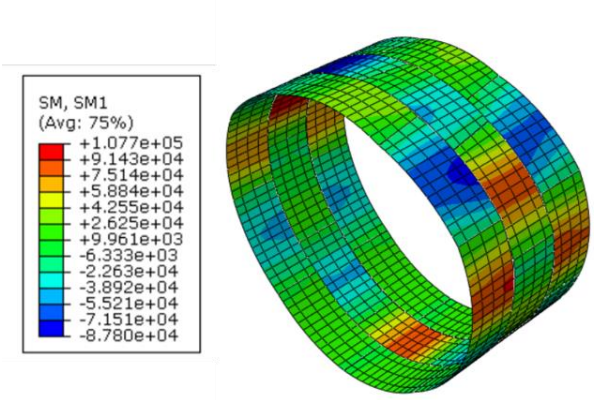

(a)

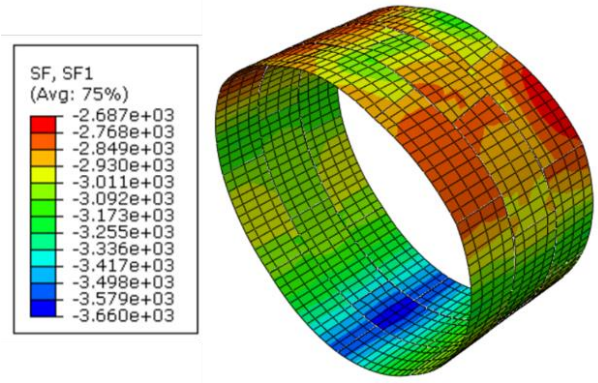

(b)

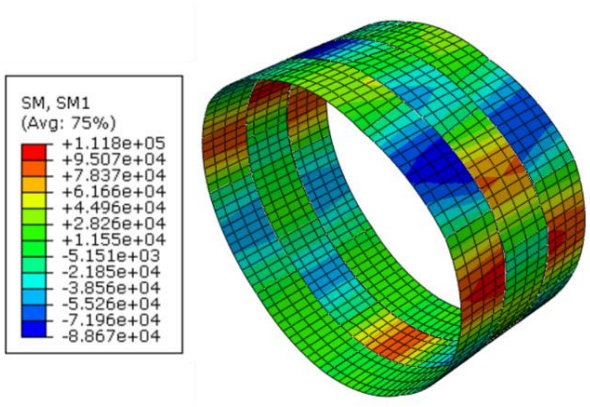

(c)

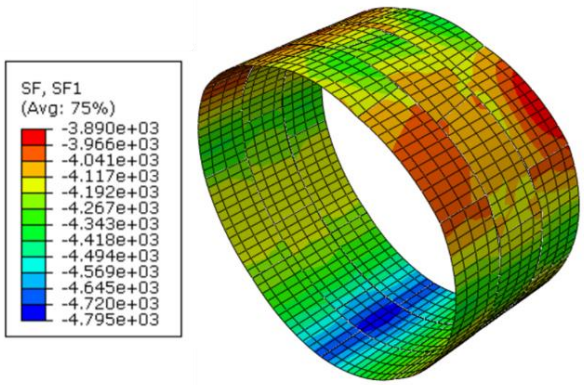

(d)

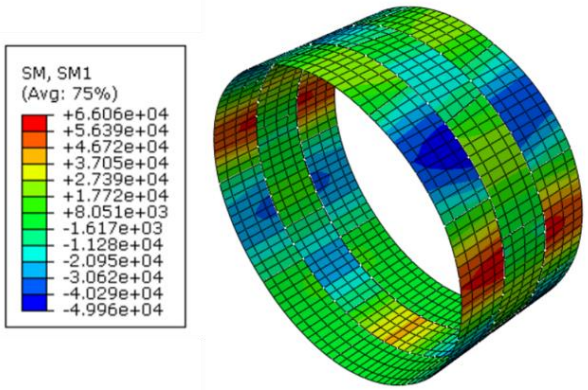

(f)

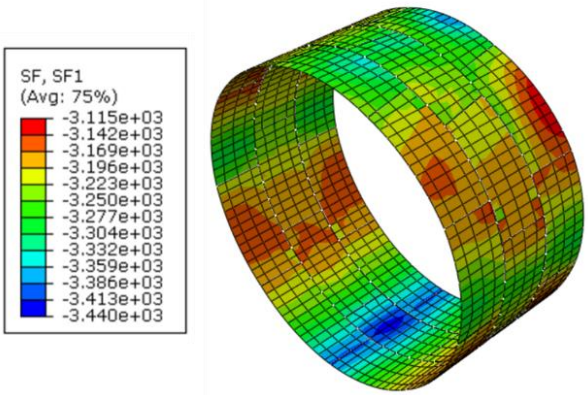

Fig. 4 Internal force distribution of structure, (a) Bending moment-0.2 MPa, (b) Axial force-0.2 MPa, (c) Bending moment-0.4 MPa, (d) Axial force-0.4 MPa, (e) Bending moment-0.9 MPa, (f) Axial force-0.9 MPa

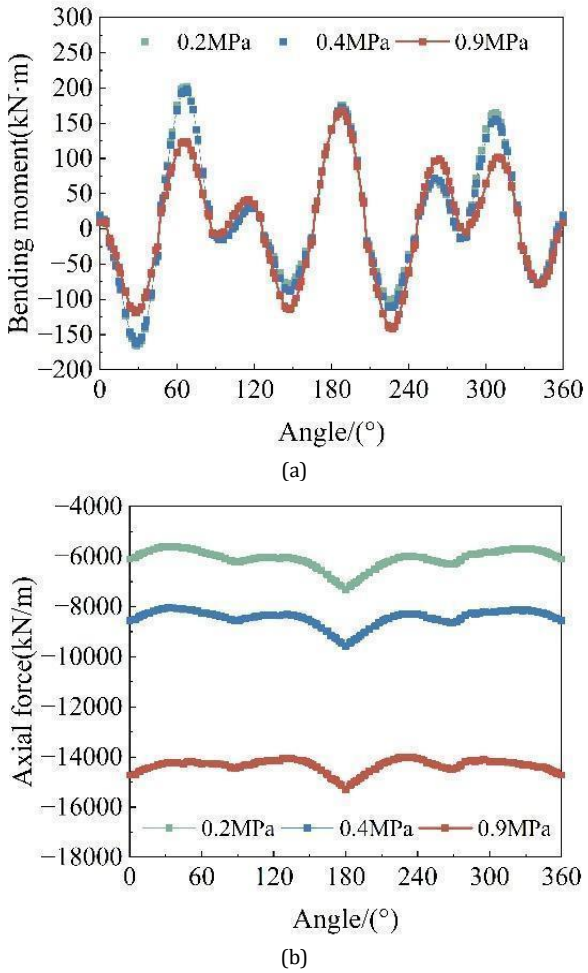

Fig. 5 Internal force of segments under different water pressures, (a) Bending moment, (b) Axial force

From the deformation cloud diagram, it is evident that the tunnel exhibits inward extrusion deformation under external loads. The staggered assembly of the segment lining leads to varying bending moments and axial forces between adjacent front and rear rings. Despite this, the axial force cloud diagram reveals a uniform transition of axial forces between the front and rear rings, indicating consistent axial force transmission along the longitudinal direction of the segments. Interestingly, under identical earth pressure and assembly methods, segments subjected to different water pressures exhibit remarkably similar distributions of bending moments and axial forces. In the analysis, it is observed that the distribution of bending moments and axial forces shows approximate symmetry along the connection line between the vault and the arch bottom. For segments under medium to low water pressure (0.2 MPa to 0.4 MPa), increasing the water pressure does not significantly alter the form or magnitude of the bending moment distribution. Notably, the segment ring positioned at the arch bottom (180°) experiences higher bending moments compared to other segments. As the external water pressure increases, the axial force in the segment also rises. Specifically, from 6000 kN/m to 8500 kN/m, there is a growth rate of 41.67%. In ultra-high water pressure conditions (0.9 MPa), the bending moment increases notably at the arch shoulder and foot, with a 60% increase near the spandrel. The axial force experiences a more pronounced increase from 0.2 MPa to 0.9 MPa, rising significantly from 6000 kN/m to 15000 kN/m, which corresponds to a 150% increase. This highlights that under ultra-high-water pressure, the predominant internal force in the segment is axial force.

From the above figure, the segment is mainly subjected to compression. To further analyze the safety and stability of the structure of the segment under different water loads, the safety factor of the concrete segment structure is analyzed in combination with Equation (3). The results at different positions are shown in the Fig. 6.

$$K = \frac{\varphi \alpha R_a bh}{N} \tag{3}$$

Where, K is the safety factor, N is the axial force, φ is the longitudinal bending coefficient, which can be taken as 1 for the tunnel lining, α is the eccentric influence coefficient of axial force, Ra is the ultimate compressive strength of concrete, b is the section width, h is the section thickness.

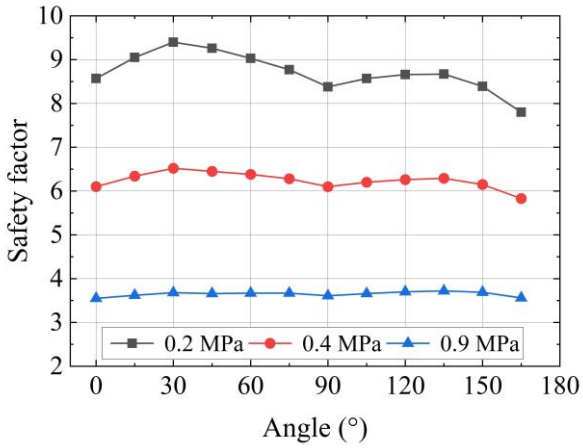

Fig. 6 Safety factor distribution of segments

The safety factor of the segment under load under different water pressures is greater than 2, indicating that the structure is safe under different working conditions. Due to the action of external water pressure, the overall load of the segment is uniform, and the corresponding safety factor is close. However, under different water pressure loads, the safety factor of the segment is quite different. The greater the external water load, the smaller the safety factor.

Analysis of mechanical properties under different assembly positions

According to the change of the assembly point position of the Pearl River Estuary Tunnel (Fig. 3), 10 assembly positions of the key blocks are selected for numerical simulation calculation. The corresponding water pressure is 0.9 MPa, and the corresponding segment displacement deformation results are shown in Fig. 7.

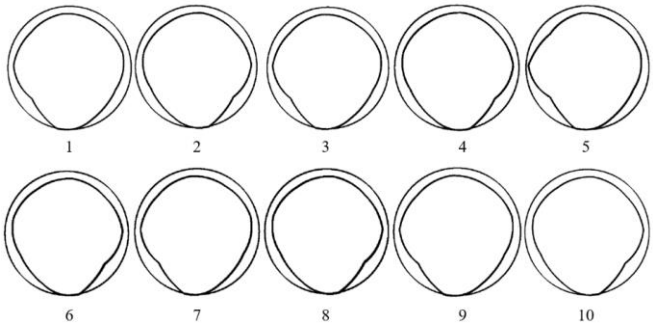

Fig. 7 Segment deformation under different assembly positions

It can be found that the overall deformation displacement of the segment is different under different assembly positions of the key block. Asymmetric deformation occurs, and the main deformation position is at the arch foot, about 4mm.At the same time, by comparing with the position of the key block in Fig. 2, the position where the maximum deformation occurs is related to the position of the segment joint at the arch bottom. When the lowest position of the joint appears on the right side, the corresponding inward displacement of the right arch foot is larger. The position of the key block in staggered assembly 5 is aligned with the arch waist, which leads to the difference in structural deformation, but the displacement value is still close.

Fig. 8 shows the internal force of the segment after partial staggered and straight assembly. By extracting the axial force and bending moment data of the middle ring, the specific results are shown in Fig. 9. There are obvious differences in the internal force distribution of segments under staggered and straight assembly. Under the straight assembly segment, the stress of the adjacent ring segment is coordinated, and the axial force and bending moment are basically the same along the longitudinal direction. Due to the discontinuity of adjacent longitudinal joints under staggered assembly, the internal load of some segments cannot be transmitted, which is more obvious in the bending moment cloud diagram.

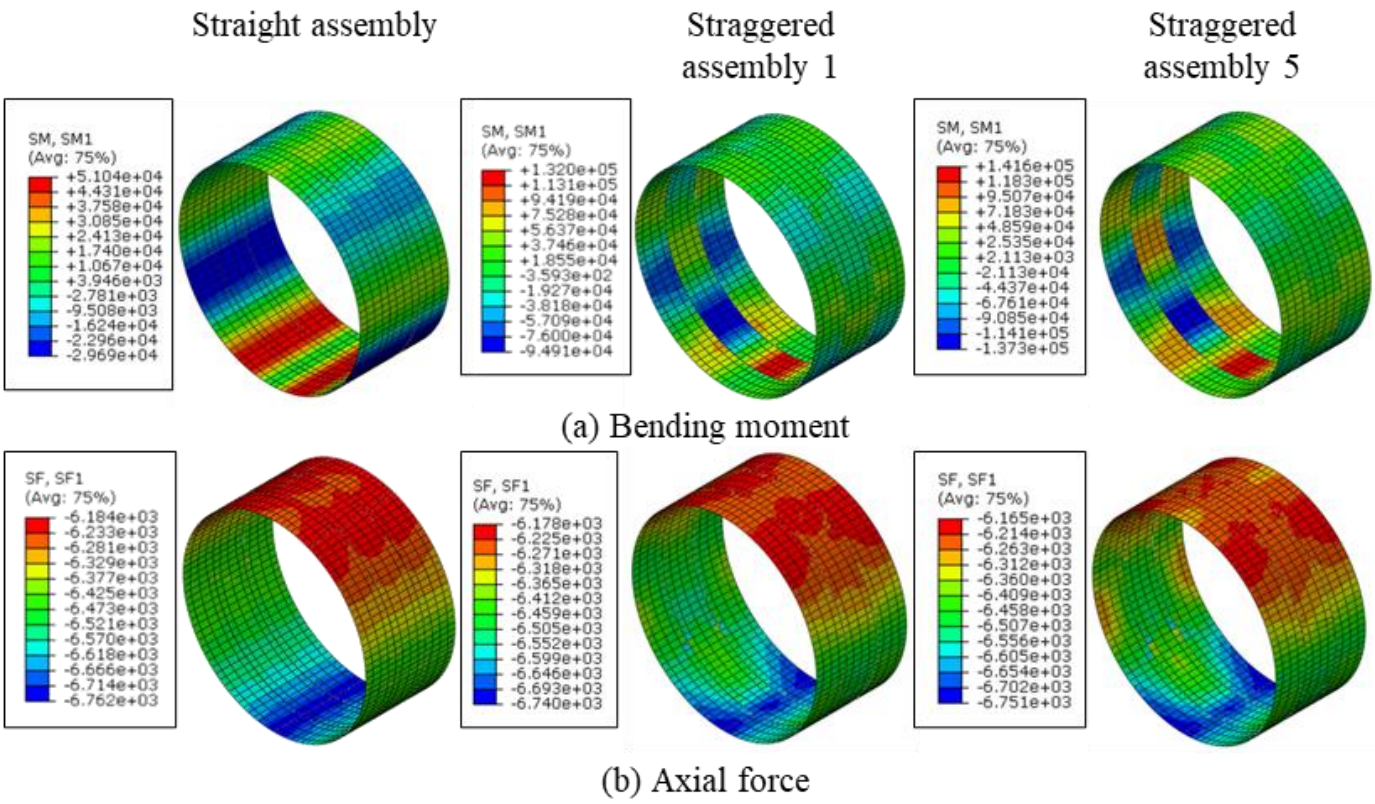

Fig. 8 The bending moment distribution of segments at different assembly positions (0.9 MPa)

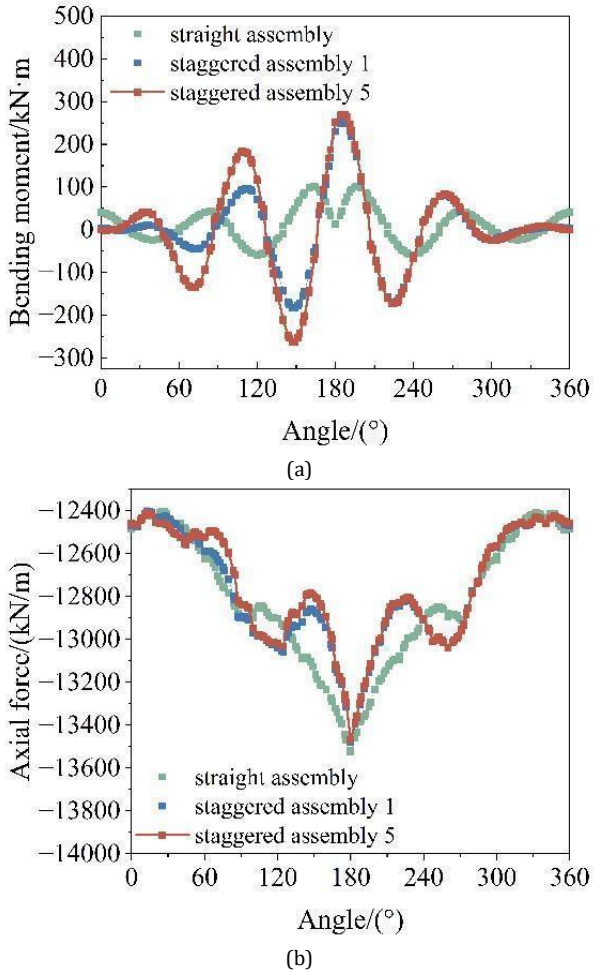

Fig. 9 Internal force of segments at different assembly positions, (a) Bending moment, (b) Axial force

Overall, the internal force distribution of different assembly methods is consistent. The peak value of positive and negative bending moment and the maximum axial force are near the invert. In terms of bending moment, the overall bending moment fluctuation of the straight assembly segment is small, and the symmetry along the connection between the vault and the arch bottom is better. However, due to the influence of staggered assembly, the structural symmetry is relatively poor, and the fluctuation range of bending moment is improved, especially near the arch foot and arch bottom. It is worth noting that the influence of different staggered assembly on the bending moment of the structure is different. The bending moment at the arch foot of staggered assembly 5 is further improved than that of staggered assembly 1. Under the influence of ultra-high-water pressure (0.9 MPa), the segment is dominated by axial force. There is little difference in axial force span between staggered and straight assembly. The minimum arch crown is 12400 kN, and the maximum arch bottom is 13500 kN. However, in the staggered assembly, the axial force fluctuation near the arch bottom is larger than that of the straight assembly segment.

4.3 Analysis of mechanical properties under different strata

According to the changes of the strata along the Pearl River Estuary Tunnel, the sandy gravel strongly weathered granite, slightly weathered gravelly sandstone and medium sand strata are selected respectively. The influence of ultra-high-water pressure on segment stress under different strata is analyzed, and the calculation results are shown in Fig.10. The axial force and bending moment data of the middle ring are extracted and listed in Fig.11.

In different strata, the response form of segment internal force to ultra-high-water pressure is similar, but the response degree is quite different. In terms of bending moment, the maximum bending moment of segments under different strata is located near the inverted arch, and its maximum value is not directly linearly related to the hardness of the stratum. At the inverted arch, the bending moment of the medium sand stratum is the largest, followed by the slightly weathered gravelly sandstone, and the sandy gravel strongly weathered granite is the smallest. In addition, near the 120° of the vaults, in the stratum with low formation strength (medium sand, sandy gravel strongly weathered granite), the bending moment oscillates obviously near the joint. In terms of axial force, different strata have a significant effect on the axial force of the segment, and the distribution form is close, and the axial force at the inverted arch is larger. The larger the soil reaction coefficient is, the more uniform the axial force of the whole segment is. This is mainly since the larger the coefficient of soil reaction, the greater the passive resistance provided by the deformed stratum of the segment, which improves the anti-deformation ability of the overall structure of the segment.

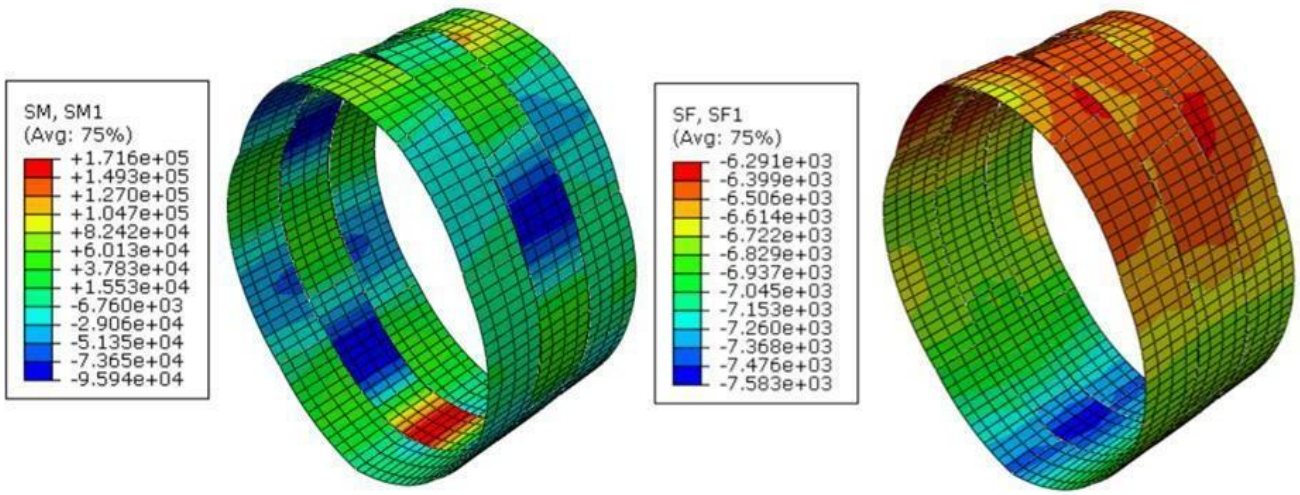

(a) (b)

Fig. 10 Internal force of segment under 0.9 MPa water pressure (medium sand stratum), (a) Bending moment, (b) Axial force

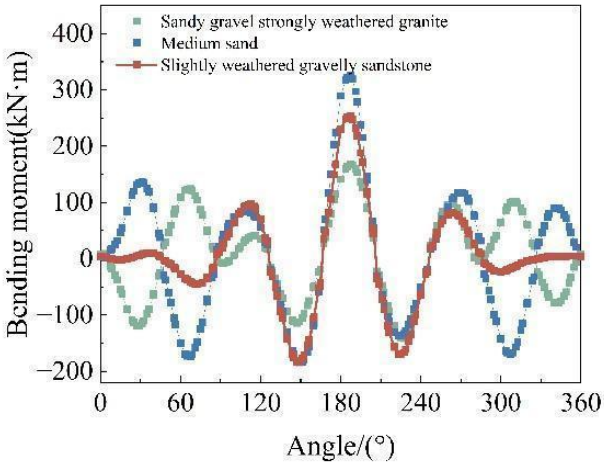

(a)

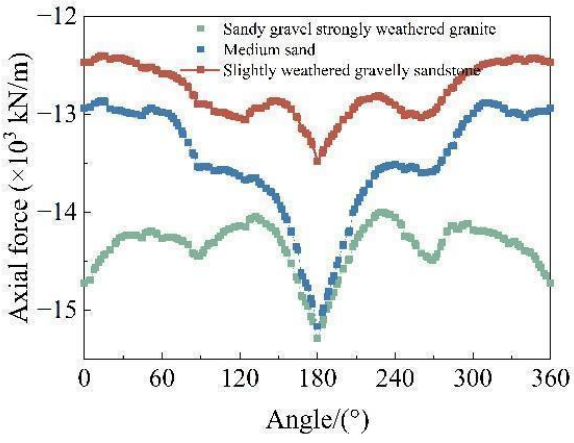

(b)

Fig. 11 Internal force of segment under different strata, (a) Bending moment, (b) Axial force

In general, the increase of the water pressure outside the stratum has a great influence on the axial force distribution of the segment. Under the same external load, different assembly methods and the position of the key block have a great influence on the bending moment distribution of the segment. The influence of different stratum environments on the axial force of the structure is higher than that of the bending moment. The above research shows that in the stratum with low stiffness of ultra-high water pressure environment, the segment is mainly axial force, and the axial force of the arch bottom is higher than that of the vault, and different staggered assembly methods have a certain influence on the bending moment distribution of the segment, which provides ideas and guidance for the subsequent segment design.

5. Conclusions

In this paper, the shell-spring model is established by ABAQUS finite element software for the submarine shield tunnel under ultra-high-water pressure. The mechanical behavior of shield tunnel segment structure under different water pressure, different key block position and different soil reaction coefficient is studied and analyzed. The main conclusions are as follows.

1. Under the same assembly segment position, with the increase of water pressure, the fluctuation of segment bending moment is small, and its axial force is greatly improved, with an increase of up to 150 %. The internal force of the segment is mainly axial force.
2. In the ultra-high water pressure environment, the corresponding position of the maximum deformation of the segment is related to the position of the segment joint at the arch bottom. Compared with the straight assembly, the axial force fluctuation near the arch bottom is larger under the staggered assembly, and the peak bending moment and the maximum axial force are near the inverted arch.
3. The stratum with different soil reaction coefficients has a great influence on the axial force and bending moment distribution of the segment. As the stratum changes from hard to soft, the bending moment oscillates more obviously near the joint in the range of 120 ° of the vault, and the axial force difference between the vault and the arch bottom of the segment is greater.
4. In the soft stratum with ultra-high-water pressure, the axial force of the segment is mainly axial force, and the axial force of the arch bottom is higher than that of the vault. In the design of segment assembly, attention should be paid to the selection of the position of the key block, the most unfavorable position should be avoided as far as possible, and the most favorable staggered assembly method under the given external load should be given priority.

Conflict of Interests

The authors declare that there is no conflict of interests regarding the publication of this paper.

Data-availability Statement

The experimental data in this paper are obtained from my own experimental results.

Acknowledgements

This research is supported in part by the National Natural Science Foundation of China (grant number: 52078428).

Reference

Arnau, O., Molins, C., 2011. Experimental and analytical study of the structural response of segmental tunnel linings based on an in-situ loading test. Part 2: Numerical simulation. Tunn. Undergr. Space Technol. 26, 778–788. https://doi.org/10.1016/j.tust.2011.04.005

Feng, K., Zhang, L., Guo, W., Yang, R., He, C., Zhang, J., 2021. Analysis on the stiffness iteration of segmental joints in segmental linings: Method and

sensitivity analysis. Tunn. Undergr. Space Technol. 115, 104043. https://doi.org/10.1016/j.tust.2021.104043

Guan, Z., Deng, T., Wang, G., Jiang, Y., 2015. Studies on the key parameters in segmental lining design. J. Rock Mech. Geotech. Eng. 7, 674–683. https://doi.org/10.1016/j.jrmge.2015.08.008

Hu Z., Luo L., Cai Z., 2005. Study on flat shell-elastic hinge-foundation model in shield tunnel. Rock Soil Mech. 1403–1408. https://doi.org/10.16285/j.rsm.2005.09.011

Huang, X., Liu, W., Zhang, Z., Wang, Q., Wang, S., Zhuang, Q., Zhu, Y., Zhang, C., 2019. Exploring the three-dimensional response of a water storage and sewage tunnel based on full-scale loading tests. Tunn. Undergr. Space Technol. 88, 156–168. https://doi.org/10.1016/j.tust.2019.03.003

Huang Z., 2007. Study on the mechanics character of shield tunnel segment with Shell-spring model (Doctoral thesis). Hohai University, NanJing, JiangSu.

Kavvadas, M., Litsas, D., Vazaios, I., Fortsakis, P., 2017. Development of a 3D finite element model for shield EPB tunnelling. Tunn. Undergr. Space Technol. 65, 22–34. https://doi.org/10.1016/j.tust.2017.02.001

Kou, L., Xiong, Z., Cui, H., Zhao, J., 2021. Study on Mechanical Characteristics of Segmental Joints of a Large-Diameter Shield Tunnel under Ultrahigh Water Pressure. Sensors 21, 8392. https://doi.org/10.3390/s21248392

Lei, M., Lin, D., Shi, C., Ma, J., Yang, W., 2018. A structural calculation model of shield tunnel segment: heterogeneous equivalent beam model. Adv. Civ. Eng. 2018. https://doi.org/10.1155/2018/9637838

Liu, J., Shi, C., Gong, C., Lei, M., Wang, Z., Peng, Z., Cao, C., 2022. Investigation of ultimate bearing capacity of shield tunnel based on concrete damage model. Tunn. Undergr. Space Technol. 125, 104510. https://doi.org/10.1016/j.tust.2022.104510

Liu, J., Shi, C., Lei, M., Wang, Z., Cao, C., Lin, Y., 2021. A study on damage mechanism modelling of shield tunnel under unloading based on damage–plasticity model of concrete. Eng. Fail. Anal. 123, 105261. https://doi.org/10.1016/j.engfailanal.2021.105261

Liu, X., Feng, K., He, C., Zhang, H., 2022. Quantitative Evaluation Index for Analysis of Assembly Effect on Shield Tunnel Segment Structures. KSCE J. Civ. Eng. 26, 4117–4127. https://doi.org/10.1007/s12205-022-1628-6

Liu, X., Jiang, Y., Li, X., Zang, Q., Yue, J., 2023. Comparative Analysis and Safety Evaluation of Shield Segment Structure Model under Surcharge Loading. Materials 16, 6806. https://doi.org/10.3390/ma16206806

Sun, J., Pei, X., Yang, C., Zhu, B., 2023. Dynamic response analysis of the process of the utility shield tunnel under-passing the operating subway tunnel. Electron. J. Struct. Eng. 23, 44–52. https://doi.org/10.56748/ejse.234433

Wang, L., Wang, Z., Li, L., Wang, J., 2011. Construction behavior simulation of a hydraulic tunnel during standpipe lifting. Tunn. Undergr. Space Technol. 26, 674–685. https://doi.org/10.1016/j.tust.2011.05.009

Xu, G., He, C., Lu, D., Wang, S., 2019. The influence of longitudinal crack on mechanical behavior of shield tunnel lining in soft-hard composite strata. Thin Walled Struct. 144, 106282. https://doi.org/10.1016/j.tws.2019.106282

Yan, Q., Zhang, C., Wu, W., Zhu, H., Yang, W., 2019. 3D Numerical Simulation of Shield Tunnel Subjected to Swelling Effect Considering the Nonlinearity of Joint Bending Stiffness. Period. Polytech. Civ. Eng. 63, 751–762. https://doi.org/10.3311/PPci.13996

Yang, F., Liu, G., Wang, Y., Yu, S., 2022. Numerical Investigation of the Segmental Lining Performance for a Shield Tunnel. KSCE J. Civ. Eng. 26, 2443–2455. https://doi.org/10.1007/s12205-022-1068-3

Zhang, L., Feng, K., He, C., Yang, W., Zhang, J., Xiao, M., 2023. Numerical investigation of the compression–bending stiffness of segmental joints with different types of joint surfaces. Tunn. Undergr. Space Technol. 132, 104898. https://doi.org/10.1016/j.tust.2022.104898

Zhang, S., Dai, L., Yuan, X., Wang, Q., Xu, J., 2023. DEM-based analysis of water inrush process of underground engineering face with intermittent joints in karst region. Electron. J. Struct. Eng. 23, 59–65. https://doi.org/10.56748/ejse.23480

Zhong, X., Zhu, W., Huang, Z., Han, Y., 2006. Effect of joint structure on joint stiffness for shield tunnel lining. Tunn. Undergr. Space Technol. 21, 406–407. https://doi.org/10.1016/j.tust.2005.12.215

Zhu H., Zhou L., Zhu J., 2019. Beam-spring generalized model for segmental lining and simulation of its nonlinear rotation. Chin. J. Geotech. Eng. 41, 1581–1590.